Investigating the effect of temperature gradient on field distribution in polymeric MV-HVDC model cable through simulation and space charge measurement

Thi Thu Nga **VU**, Gilbert **TEYSSEDRE**, Bertrand **VISSOUVANADIN,** Sèverine **LEROY**, Christian **LAURENT;** Laboratoire Plasma et Conversion d'Energie, Université P Sabatier, Bat 3R3, 118 Route de Narbonne, 31062 Toulouse, (France), vu@laplace.univ-tlse.fr, gilbert.teyssedre@laplace.univ-tlse.fr, bertrand.vissouvanadin@laplace.univ-tlse.fr, severine.leroy@laplace.univ-tlse.fr, christian.laurent@laplace.univ-tlse.fr.

Mohamed **MAMMERI**, Isabelle **DENIZET;** SilecCable, rue de Varennes Prolongée, 77876 Montereau Cedex, (France), mohamed.mammeri@sileccable.com, isabelle.denizet@sileccable.com.

ABSTRACT

One of the major issues in the development of synthetic insulation HVDC cables is space charge accumulation in the insulation and the consequent distortion of the electric field under voltage. In addition, the current flow through the conductor is a source of heat which results in a temperature gradient and therefore a conductivity gradient along the cable insulation radius because the electrical conductivity of polymeric materials is mostly an increasing function of temperature. Also, the conductivity is field dependent, in a field range covering the design field of DC cables. To satisfy a constant current flow across the cable radius under steady state condition, such situation necessarily results in a redistribution of the electric field and therefore an accumulation of space charge within the bulk of the insulation. The aim of the present contribution is to investigate the influence of temperature gradient on the accumulation of space charge and distribution of electric field in polymeric MV-HVDC model cable through simulation and measurements.

KEYWORDS

Space charge, HVDC cable, electric field distribution, temperature gradient.

INTRODUCTION

With the advantages of using HVDC system compared to HVAC system, especially for long-distance transmissions [1], HVDC cables are increasingly used and gradually replace HVAC cables for electrical energy transport. However, space charge accumulation in HVDC cables under various temperatures and applied fields is the major problem when in service. Indeed, when space charge density is sufficiently high, the local field strength may exceed the breakdown strength of the dielectric, leading to premature failure. This is why space charge has been extensively studied since over the last 20 years for the development of polymeric-type DC cable systems.

Amongst the different mechanisms of space charge accumulation the effect of temperature gradient on field distortion has been the subject of many studies. Interest on the subject begins with the work of McAllister et al. who considered space charge accumulation phenomenon from the macroscopic point of view using electromagnetic field theory [2]. In their work, charges accumulation was analysed as a consequence of a non-uniform conductivity. An expression of steady-state space charge distribution in polymeric DC cable has been proposed assuming that the conductivity increases exponentially with temperature and through a power law with field strength.

Jeroense and Morshuis [3] have computed space charge and field distributions in the case of paper-insulated HVDC cables for different stages both for transient and steady state conditions. The insulating material conductivity was assumed to depend exponentially on temperature and field. By disregarding the field dependency of conductivity σ, an analytical expression of field distribution and resistance per meter cable was derived. In this particular case, the field distribution is mainly governed by the temperature drop across the cable radius. It has been shown that for a sufficiently large temperature drop, the field strength is inverted with respect to the capacitive field [3]. Indeed, with the above hypotheses (temperature dependent σ), using Maxwell's equations, it can be shown that in steady state conditions the field distribution inside the dielectric in cylindrical geometry is given by [4]

$$E(r) = E_0 \frac{r_0 \sigma_0}{r \sigma(r)} \qquad [1]$$

where E_0 and σ_0 are the field and conductivity at reference position r_0. The space charge density associated with a non-uniform conductivity is of the form:

$$\rho_{tg} = -E(r) \cdot \frac{\varepsilon_0 \varepsilon_r}{\sigma(r)} \frac{d\sigma(r)}{dr} \qquad [2]$$

For σ(T) following an Arrhenius dependence with temperature with E_a as activation energy,

$$\rho_{tg}(r) = -\varepsilon_0 \varepsilon_r E(r) \cdot \frac{E_a}{kT^2} \frac{dT}{dr} \qquad [3]$$

where T is the temperature. It can be shown from Eq (1) that if the conductivity varies with radius faster than an hyperbolic law does, then the field increases from inner to outer screen. From Eq. 2 and 3, it can be seen that the sign of the space charge density associated with conductivity gradient is directly linked to dσ/dr: for a negative voltage applied to the conductor (E>0), a negative space charge is predicted in case of temperature gradient with conductivity increasing from inner to screen (Eq.3) whereas space charge is positive if the conductivity gradient is linked to a conductivity increasing with field (hence decreasing as *r* increases, cf. Eq.2): In a situation where the two processes are combined, the sign of the space charge is undetermined a priori.

Boggs et al. [5] recently investigated the behaviour of the resistive field distribution under non-uniform temperature conditions for two categories of insulating polymers of which the conductivity has different thermal activation energy. They demonstrated the importance of using materials having low E_a and large field-dependence of

conductivity to control the electric field distribution under conditions of large thermal gradients.

The field distribution in HVDC cable is controlled by the insulating material conductivity which is a strong function of temperature and can substantially vary with electric field. However, the dependency of conductivity with field and temperature is specific to each material. Besides, space charge accumulation processes may occur without necessarily being linked to the temperature gradient in the material. This further complicates the predicted field distribution. The purpose of this contribution is to compare predicted field distribution in cable models based on conductivity measurements taken on flat specimen to actual field distributions obtained by the pulsed electroacoustic method on cable samples.

In the purpose of investigating the evolution of conductivity of cable materials with field and temperature, current-voltage measurements have been carried out on XLPE plaque samples under various conditions of temperatures and voltages. Then, functional variation of conductivity with temperature and electric field is derived from the fit of the quasi-stationary charging currents (conduction currents). From the established semi-empirical conductivity model, space charge distribution has been computed using Comsol® within XLPE MV-model cable in presence or absence of a thermal gradient. Space charge measurements have been also carried out on MV-HVDC model cables and results are discussed and compared to those obtained with simulation.

EXPERIMENTAL

Conductivity measurements

Conductivity measurements are performed in the form of plaques of cross-linked polyethylene (XLPE) with thicknesses varying from 500 µm to 600 µm. Samples were kept sealed in aluminium bags after cross-linking.

Both faces of samples were gold-metalized by sputtering to form 50 mm-diameter electrodes. A silicone ribbon was laid at the periphery of the electrodes to avoid edge phenomena. Measurements were performed in air at temperatures ranging from 0℃ to 90℃ by step of 10 °. The temperature was controlled by a thermo stated sample holder. To avoid possible memory effects, a new sample has been used for each value of temperature. Charging currents have been measured for 1 hour for 10 values of DC fields varying from 2 to 25 kV/mm under isothermal condition. Depolarization was applied for 1h after each volt-on step. Current values were recorded every 2 seconds all along the measurements.

Space charge measurement

Tested samples are sections of Medium Voltage –MV-XLPE cables, about 3 m long, with 4.5mm thick insulation (inner and outer radiuses are 5 mm and 9.5 mm, respectively). The conductor diameter is 8 mm. The inner and outer semicon (SC) thicknesses are 1 and 0.5 mm. Space charge measurements were realized using the pulse-electro-acoustic (PEA) method through the configuration represented in Fig. 1. The PEA-Cable device was provided by TechImp®, Italy. The cable is fixed to the PEA cell by means of a cable holder at the measuring point, which guarantees a good acoustic contact between outer SC and aluminium electrode of the measuring device. The pulse voltage is injected via the outer SC of the cable. The outer SC is removed over a length of 5 cm between the measuring location and the region where the pulse is applied. In this way, the cable itself acts as a decoupling capacitor. The DC voltage supplied by a high voltage generator is applied at inner conductor via a Rogowsky electrode avoiding corona discharges at the cable connection.

In this work, two different test conditions have been considered, being room temperature and 11℃ temperature drop across the insulation. For the former condition, the cable was kept at ambient while for the second, temperatures at the inner and outer SC shields were set to 51℃ and 40℃ respectively. To achieve such a temperature drop across the cable insulation, the test sample was connected in a loop using a screw connector to allow an ac current induced by a transformer to flow in the cable core. The conductor was heated with a current of 200 A while the surface of the cable was kept in air. It is noteworthy that in this way the steady state temperature at the cable surface is influenced by the environment condition. In particular, the PEA cell tends to reduce the temperature at the cable surface since the aluminium shield of the PEA cell acts, besides as delay line, as a heat dissipater. Hence, the temperature drop is expected to be higher at the measuring location than somewhere else along the cable suspended in air. In our case, after 100 minutes of current injection, the cable surface temperature was in steady state at 40^0C. The heat flow over the cable radius being conservative under steady state, the temperature at the inner conductor could be estimated from the surface temperature (measured), the Joule losses ($R.I^2$) in the inner conductor and the thermal resistance of the cable insulation.
A DC negative voltage of -40kV was applied at the inner conductor of the cable for 7 hours followed by 1 hour of depolarization. Pulse voltage was applied using a 5kV/30ns/10kHz pulse generator. For the present measurements, the pulse frequency was limited to 5kHz.

Raw PEA signals were recorded and averaged every 200 seconds all along the voltage cycle. They were subsequently treated by the deconvolution technique as detailed in the following subsection.

Deconvolution of PEA signals

Since the PEA method relies on the generation of

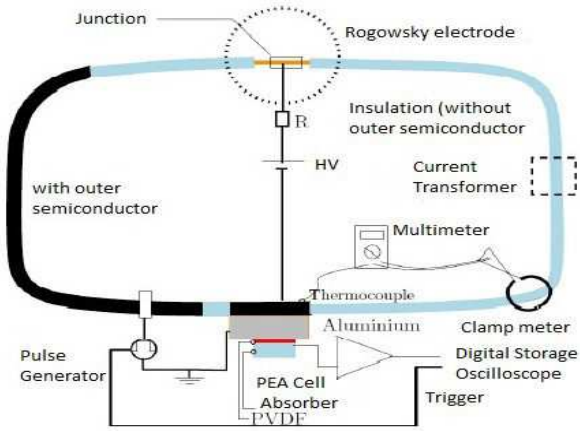

Fig. 1: Schematic representation of the PEA Cable system.

electrostatic forces through interaction between embedded charges and the external pulse field [6], acoustic wave propagation in the direction of the piezoelectric sensor mostly suffers from attenuation and dispersion especially when dealing with relatively thick insulating materials as for MV-cable samples. Furthermore both generation and propagation of waves are affected by the geometry of the cable. Especially, the contribution to the PEA signals of the electrostrictive force – caused by the strain-induced variation of permittivity – can no longer be ignored as for plaque samples [7]. The deconvolution method used in this work aims at correcting overall effects encountered in cable geometry, namely attenuation, dispersion, electrostriction and non-flat frequency response of the PEA set-up (sensor + voltage pulse). For sake of simplicity, the deconvolution is presented as a flow chart (see Fig. 2) and the different steps shall be briefly exposed. The reader may refer to [8] for more details about the method.

The deconvolution of raw PEA signal requires an accurate description of the full system which consists of the measurement set-up and the tested cable. Calibration procedure, which consists in applying a given DC voltage (U_{cal}) and acquiring the corresponding PEA signal, is used to derive the global system transfer function H_{syst} (r,f). The latter is obtained by multiplying the position-dependant cable transfer function (g(r,f))) by the set-up transfer function (H_{setup}). In the cable transfer function g(r,f)) are taken into consideration the effects of attenuation and dispersion of acoustic waves in the cable while H_{setup} models the non flat frequency response of the detection and conditioning circuit. Material transfer function g(r,t) is computed from the frequency-dependent wave attenuation (α(f)) and velocity (c(f)). These quantities are derived from the calibration signals spectra generated by the capacitive charges on outer and inner electrodes. H_{setup} is obtained normalizing the spectrum of the first part of the calibration signal with the calibration voltage U_{cal}. The generated pressure distribution across the cable m(r) is computed from the Inverse Fourier Transform (IFFT) of the spectral ratio between the PEA signal V_{PEA}(f) and the system transfer function H_{syst} (r,f). Electric field E(r) and space charge ρ(r) profiles are subsequently derived from the pressure distribution.

The current deconvolution method is potentially applicable in any type of cable. As illustrations, we show in Fig. 3 results obtained with two types of XLPE insulated cables: medium voltage (MV) and mini-cable of which insulating thicknesses are respectively 4.5 mm and 1.5 mm. For the MV cable (Fig. 3.a), measurements were carried out at room temperature with successive polarization-depolarization steps in which voltages applied to the core conductor were -40 and -80 kV. Polarization / depolarization lasted for 3 / 1 h. For mini cables (Fig. 3.b), measurements were carried out in presence of 10℃ temperature gradient. The cable core was heated to 70℃ while the external cable surface was at 60℃. One c ycle of polarization/depolarization were applied. The polarization stage was -55 kV for 4 h; depolarization was for 4 h.

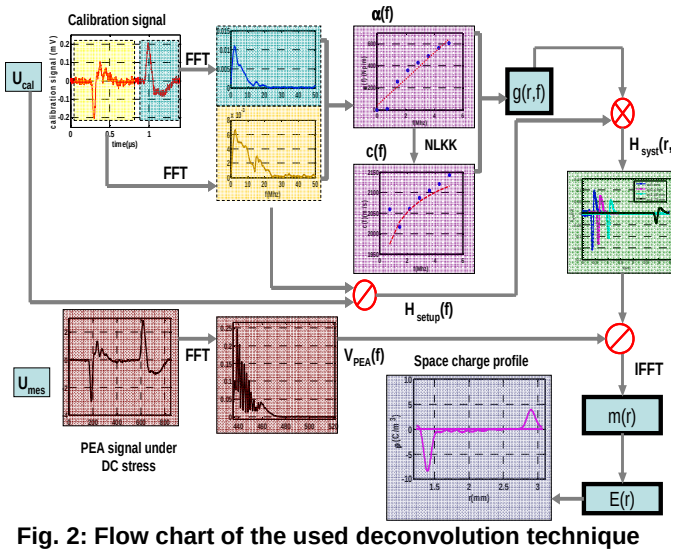

Fig. 2: Flow chart of the used deconvolution technique

The spatial evolution of space charge density is represented in form of cartography. This is a convenient way to follow the processes of charges accumulation and relaxation in the material. In this representation, the time is given on X-axis; the radius is along the vertical axis (anode to the top, cathode to the bottom) and colour scales represent charge density, negative and positive polarity being represented by cool and warm colours respectively. In the MV cable, the cartography of space charge density (Fig. 3.a) highlights the slow transit of negative charges from the inner to the outer electrode. In the mini cable (Fig. 3.b), it has been observed that a fast transit of negative charges front occurs during the first 20 min of polarization. Positive charges injection occurred at the anode; however these charges stay trapped close to the electrode. Space charge pattern also reveals that the bulk of mini cable is mainly occupied by negative charges arising from injection process at the cathode.

SIMULATION RESULTS BASED ON CONDUCTIVITY DATA

DC conductivity of insulating polymers is generally temperature and electric field-dependent. Such a coupling

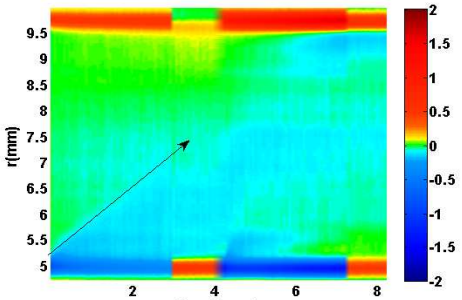

(a) MV-cable, -40kV and -80kV at 22℃

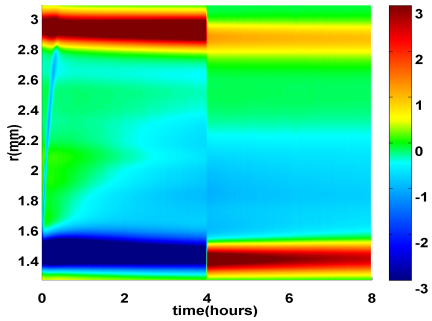

(b) Mini-cable, -55kV at temperature gradient

Fig. 3: Examples of space charge cartographies obtained using the PEA-Cable system. The colour bar represents charge densities in C/m³

between field and conductivity makes the assessment of the electric field distribution across the cable radius rather complex analytically even with assuming steady state condition. This difficulty is overcome when using numerical solver to compute the field distribution under temperature gradient condition. Another advantage of using numerical solver is the possibility of obtaining solutions both under transient and steady state conditions.

Fig. 4 shows the field dependence of quasi steady-state current obtained on XLPE plaque samples for different temperatures. It can be observed that for all temperatures, the current increases with field with a slope substantially higher than 1, even at low temperature. Therefore, the conductivity seems always field-dependent. The current increases by over two orders of magnitude for the 50℃ temperature variation shown here.

Through fitting of these current measurement data, an expression of conductivity vs. temperature and electric field has been established. It is expressed as [9]:

$$\sigma(T,E) = A.\exp(\frac{-E_a}{k_B T}).\sinh(B(T).E).E^{\alpha} \qquad [4]$$

where A and α are constants, E_a is the thermal activation energy, k_B is the Boltzmann's constant, and B = $aT+b$ is a temperature-dependent coefficient to account for the change in threshold field versus temperature. Coefficients for equation (4) are as follows (with σ in S/m, E in V/m, T in K): A=0.8 (SI), Ea=1 eV, a=0 and b= 10^{-2} (T<313K), a= 1.3 10^{-9} and b=3.36 10^{-7} (T≥313K).

The above semi-empirical expression of conductivity has been implemented in COMSOL to compute space charge and electric field distribution in MV-cable in absence or presence of a thermal gradient. We consider the case of -40 kV applied to the core conductor of the cable (inner electrode). The outer electrode (outer SC) is set to 0V. We have represented in Fig. 5 the predicted change in field distribution across the cable radius during 7 h of voltage-on in ambient condition (22℃). In these conditions, the electric field does not considerably change in time; the distribution stays similar to that of the Laplace field (with constant conductivity). The field magnitude roughly decreases and increases in time at the inner and the outer electrodes, respectively. This is due to a higher value of the field in the vicinity of the inner conductor at the beginning of polarization, resulting in a higher conductivity (owing to eq. 4). To converge to the steady state regime, in which σ(r).E(r).r is constant due to current flux conservation, the field strength at this location

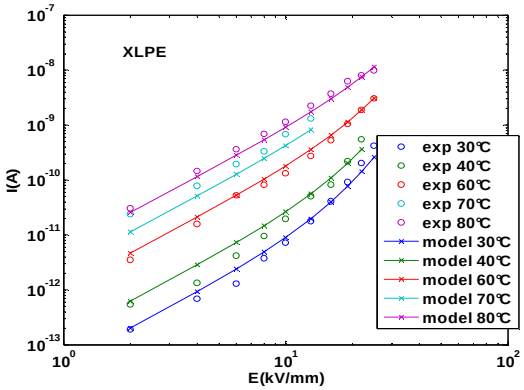

Fig. 4: Experimental current-field plots of XLPE at different temperatures. Solid lines are fits to Eq.4.

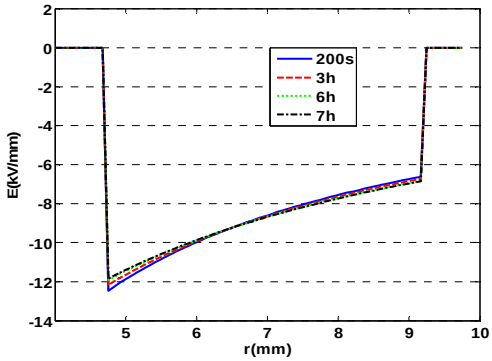

Fig. 5: Computed field distribution at different times in model cable stressed under -40kV at 22℃.

decreases and so does the conductivity. Conversely, close to the outer electrode, since the conductivity of the insulation is initially lower (the initial field being lower) the field is increasing in time. After 7 h of polarization, the field values were estimated to 11.8 kV/mm and 6.8 kV/mm at inner and outer SC respectively. For the present conditions, space charge density (negative, not shown here) was very low; the highest value – found at the inner SC after 7 h of charging – was of the order of -10 mC/m^3.

Fig. 6 shows space charge and electric field profiles – obtained from simulation – at various times under -40 kV in presence of 11℃ thermal gradient (40℃ at the o uter SC and 51℃ at the inner SC). From Fig. 6a, it can be observed that negative charges are rapidly accumulating adjacent to inner conductor during the first hour of polarization. After 3 h, their density varies from -40 mC/m^3 to -16 mC/m^3 along the cable radius. Then, the space charge density begins to slightly decline at inner electrode while at outer electrode it is still increasing. As a consequence, the electric field decreases and increases in time respectively at the inner and outer conductor and the field distribution is inverted (in respect to the initial Laplacian field) after about 3 h of polarization (see Fig. 6b). Furthermore, it can be noticed that there is a position in the insulation bulk (located at about 2 mm from the inner conductor) where the field magnitude remains nearly unchanged during the polarization.

Hence, the presence of 11℃ temperature drop within the XLPE insulation of the cable induces a drastic change compared with the previous situation (homogeneous temperature). Indeed, a higher amount of negative charges is expected to accumulate in the bulk of the insulating polymer when temperature gradient takes place between the inner and outer conductor. This is because the temperature drop within the insulation results in a higher gradient of conductivity along the cable radius leading to higher distortion of field compared to the situation where the temperature is homogeneous for which only the field contributes to the change in the conductivity along the cable radius.

SPACE CHARGE MEASUREMENTS

Space charge and electric field distributions obtained under -40 kV at room temperature are shown in Fig. 7. Space charge profiles (Fig. 7a) show positive charges accumulated in the bulk of the sample at 1-2 mm from anode and heterocharges build up at the close vicinity of the anode immediately after voltage application. These charge densities are small, being less than 80 mC/m³, and

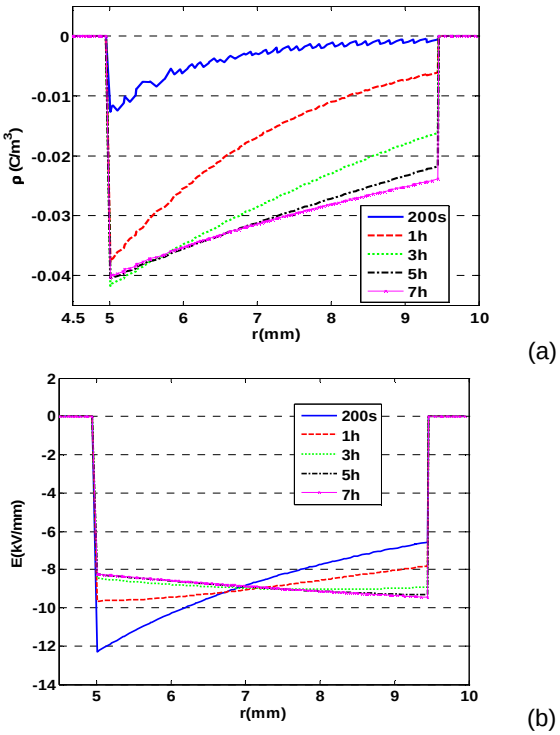

Fig. 6: Computed space charge (a) and field (b) distribution at different times in MV cable under -40kV in presence of thermal gradient.

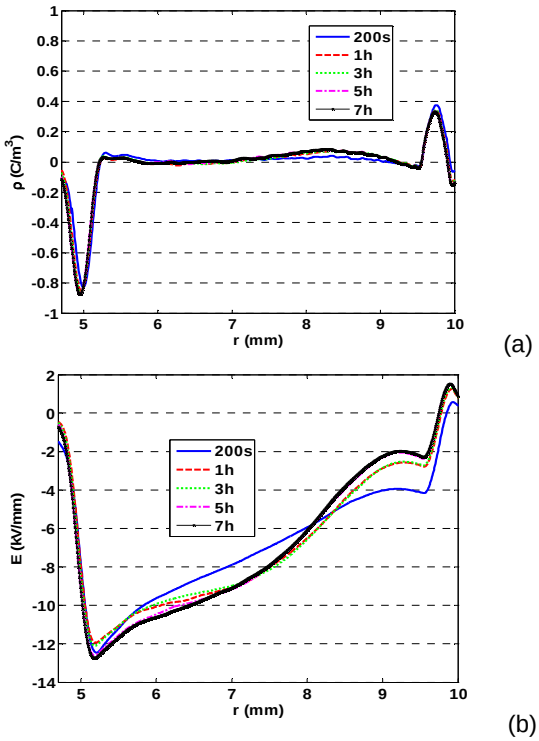

Fig. 7: Space charge (a) and electric field (b) profiles vs. time in MV cable under -40kV at 22℃.

the steady state of space charge accumulation process seems reached after 5 h of poling. During polarization, the electric field profiles slightly deviate from the initial Laplacian field distribution due to space charge accumulation (Fig. 7b). After 7 h of polarization, the electric fields to the inner and outer electrodes are found to be approximately 13 kV/mm and 2 kV/mm. The respective field values short after voltage application were 12.8 kV/mm and 4 kV/mm so that in this case the maximum stress remains located to the inner SC.

Fig. 8 shows the results when a temperature gradient of 11℃ is applied across the cable insulation. In Fig . 8a, we observe that negative charges are accumulating in the middle of the cable insulation during the first hour of poling. Then, negative charges tend to move progressively towards the anode forming heterocharges after 7 h of polarization. The density of negative charges in insulation bulk is approximately -80 mC/m^3. Fig. 8b reports changes in field profile during voltage-on step. It clearly shows the respective decrease and increase of field strength at the inner and outer SC due to the build-up of negative charges in the bulk of the insulation. After 7 h of polarization, the highest stress is located at the outer electrode and is estimated to about 10.5 kV/mm: the field is approximately multiplied by a factor 2 during the polarization stage at the outer electrode. Conversely, at the inner electrode, the field strength is approximately halved in respect to its initial value. Finally, the lowest field strength appears to be located at the middle of insulation. This is due to the configuration of the negative charges, which are accumulated adjacent to the anode (Fig 8a), and the diverging nature of field in coaxial geometry.

Comparing experimental results obtained in absence and in presence of a temperature gradient across the insulation of the cable, it is clear that the thermal gradient has a strong effect on charges accumulation and field distribution in the cable. Without thermal gradient, a small quantity of positive charges are accumulating in the bulk of cable insulation while in presence of temperature gradient negative charges are building up adjacent to the anode forming heterocharges.

DISCUSSION

Questions that can be raised from the present approach concern the capability of conductivity measurements to predict field distortion inside HVDC cables. Deviations between model and experiments may arise for different reasons: First, conductivity measurements taken on flat specimen, with gold electrodes may not be representative of cable conditions as processing/crosslinking conditions of samples are different, the outgassing degree is different and electrodes are of different nature. Second, only some processes of charge build up are considered, i.e. the non-homogeneous conductivity due to field and temperature gradients encountered in the cable geometry. In flat geometry as example it is well know that space charge builds up, which would not be expected with only a temperature and field dependent conductivity: this is due to space charge processes linked for example to ionic species formation and drift or to space charge limited conduction. It is therefore interesting to evaluate to what extent the modelled field distribution is verified by experiments issued from space charge distribution measurements.

In absence of thermal gradient, both simulation and measurement show a low amount of accumulated space charge and therefore a weak distortion of electric field. However, it can be noted that the amount and polarity of charges are quite different. Experimental charge density was about twice that predicted from simulation. This difference indicates that other mechanisms of space

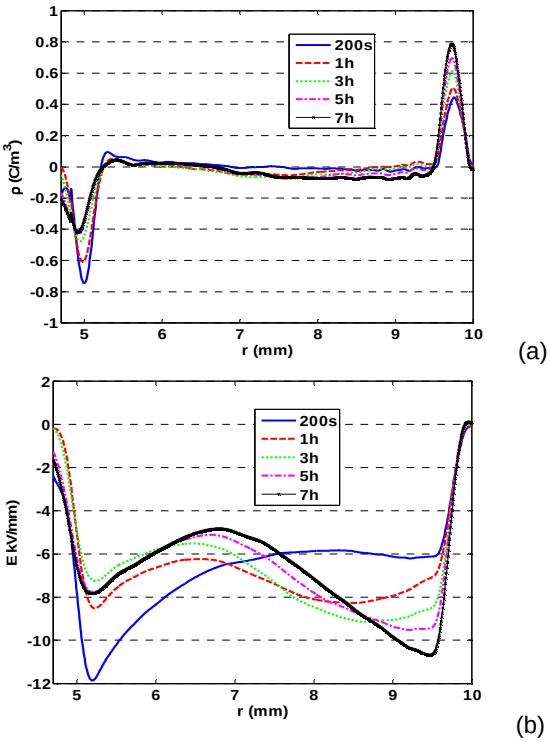

Fig. 8: Space charge (a) and electric field (b) distribution in model cable at different times under -40kV in presence of thermal gradient.

charge generation such as injection or field-assisted impurity dissociation (which are not taken into account in the simulation) actually take place in addition to charge accumulation due to the conductivity gradient.

In presence of temperature gradient, the polarity of charges are similar for both experiments and simulation. However, simulation predicts a quasi-uniform distribution of charges within the insulation bulk with an average density of about -30 mC/m^3 while experimental results show that charges accumulate preferentially adjacent to the anode with a higher density (about -80 mC/m^3) which leads to a difference in the distribution of field. For simulation, the field increases monotonically from the inner to the outer conductor after 7 hours of polarization under -40 kV while experimental results indicate that the minimum of field occurs in the bulk of insulation. Assumption made on the nature of electrodes is likely to be at the origin of this difference. With regard to simulation, charges are computed assuming perfect ohmic contacts meaning that charges can freely enter or leave the insulating material. However, the formation of heterocharges observed experimentally seems to indicate the possible presence of a potential barrier toward charge extraction at the external SC. Nonetheless, one can obtain a rather good estimation of electrode fields during steady state using simulation based on space charge-induced conductivity gradient.

A last comment concerns the kinetics to approach the steady state regime. In the configuration of temperature gradient, the time constant for charge redistribution ($\tau=\varepsilon/\sigma$) is of the order of 3h at 50℃ (inner SC) and 6.7h at 40℃ (outer SC) (both are given for a field of 10kV/m m). Referring to the field distribution of Fig.8b, it seems that effectively the field distribution tends to a stable distribution after polarization for 7h.

CONCLUSION

An expression of conductivity versus temperature and electric field has been derived based on charging current measurements on crosslinked polyethylene constituting the insulation of a MV-HVDC cable. The time dependence of the field strength distribution in the MV cable insulation has been predicted in absence or presence of a temperature gradient. Simulated charge and field distributions are compared to those obtained experimentally by PEA method under -40kV applied to the conductor in absence and presence of a thermal gradient. The results show that with temperature gradient across the radius of the cable insulation, space charge builds up within the insulation due to the non-homogeneity of the insulation conductivity. The field redistribution is very significant, the maximum in local field moving to the outer SC screen, as expected from the simulation. It is shown that the field distortion is ever pronounced than predicted due to heterocharge build close to the outer SC screen.

REFERENCES

[1] Europacable Report, 2011, "An Introduction to High Voltage Direct Current (HVDC) Underground Cables", 13p. cf. *http://www.europacable.com*

[2] I.W. McAllister, G.C. Crichton, A. Pedersen, 1994, "Charge Accumulation in DC Cables: A Macroscopic Approach", Proc. IEEE-ISEIM, pp. 212-216.

[3] M. Jeroense, P.H.F. Morshuis, 1998, "Electric Fields in HVDC Paper-Insulated Cables", IEEE Trans. Dielectr. Electr. Insul., vol. 5, pp. 225-236.

[4] D. Fabiani *et al.*, 2008, "HVDC Cable Design and Space Charge Accumulation. Part 3: Effect of Temperature Gradient", IEEE Electr. Insul. Mag., vol. 24, n° 2, p. 5-14.

[5] S. Boggs, H. Dwight, J. Hjerrild, J.T. Holbol, M. Henriksen, 2001, "Effect of Insulation Properties on the Field Grading of Solid Dielectric DC Cable", IEEE Trans. Power Deliv., vol. 16, pp. 456-462.

[6] T. Maeno, T. Futami, H. Kushibe, T. Takada, C.M. Cooke, 1988, "Measurement of Spatial Charge Distribution in Thick Dielectrics Using the Pulsed Electroacoustic Method", IEEE Trans. Electr. Insul., vol. 23, pp. 433-439.

[7] S. Holé, 2000, "Influence of Divergent Electric Fields on Space-charge Distribution Measurements by Elastic Methods", Phys. Rev. B, vol. 61, pp. 13528-39.

[8] B. Vissouvanadin, T.T.N. Vu, L. Berquez, S. Le Roy, G. Teyssedre, C. Laurent, "Deconvolution Techniques for Space Charge Recovery Using Pulsed Electroacoustic Method in Coaxial Geometry", accepted, IEEE Trans. Dielectr. Electr. Insul.

[9] T.T.N. Vu, G. Teyssedre, B. Vissouvanadin, S. Le Roy, C. Laurent, M. Mammeri, I. Denizet, 2013, "Electric field profile measurement and modeling in multi-dielectrics for HVDC application", Proc. IEEE-ICSD, pp. 413-416.